

# Estimating Strain and Stress in Oriented Rock Cores Using a Diametral Deviation Method

Monte Hieb, PE

West Virginia Office of Miners' Health, Safety, and Training

## ABSTRACT

A practical core-based method for estimating in-situ stress was tested using 360-degree measurements of rock core diameter in a laboratory setting. In several mining districts across West Virginia rock cores were recovered from exploration core holes and oriented using an acoustic televiewer (ATV) summary log. Measurements of diametral variation were performed at 0.1-foot depth intervals using a benchtop device comprised of a pair of diametrically-opposed contact digital indicator gages working in tandem. The diametral profiles were evaluated to determine strain direction and strain magnitude. Stress magnitudes were calculated when values for Young's Modulus, and Poisson's Ratio were available. Stress direction results are compared to other stress determination methods, including downhole overcores, drilling-induced fractures, and borehole breakouts. The testing and analytical methods used are similar to the Diametrical Core Deformation Analysis (DCDA) method (Ito, T., Funato, A., Shono, T., 2012), but with a number of important improvements. The diametral deviation method presented here was found to be a practical working approach for characterizing the local in situ horizontal stress field, although aspects of it are still considered to be experimental.

## INTRODUCTION

Knowledge of the horizontal stress field is essential to mine planning and design, and exploration by wireline core drilling methods is an essential tool in that process. Ordinarily, operators will box and save only a small number of cores for analysis, usually from core runs immediately above and below the drilling target. However, the remaining cores are a valuable resource for characterizing the state of in situ stress based on new technology that non-destructively determines the direction and magnitude of horizontal strain and stress through an analysis of its diametral deviation.

This paper is part of a five-year study performed in cooperation with mine operators across West Virginia. Over 900 feet of core were tested from 21 core holes and approximately 6,000 useable strain profiles were obtained. Statistically robust datasets were compiled, from which strain and stress estimates were performed and those results

are compared here against other conventional stress methods and indicators. The study shows that in sedimentary rocks in certain locations of West Virginia the direction of maximum horizontal stress ( $S_H$ ) varies with general rock strength, for which lithology is an indicator. Rock cores from eight (8) mine sites were studied; their general locations are indicated in **Figure 1**. Discussion in this paper cites specific results from test locations 2, 3, 4 and 5, but all sites contributed to general knowledge and method development.

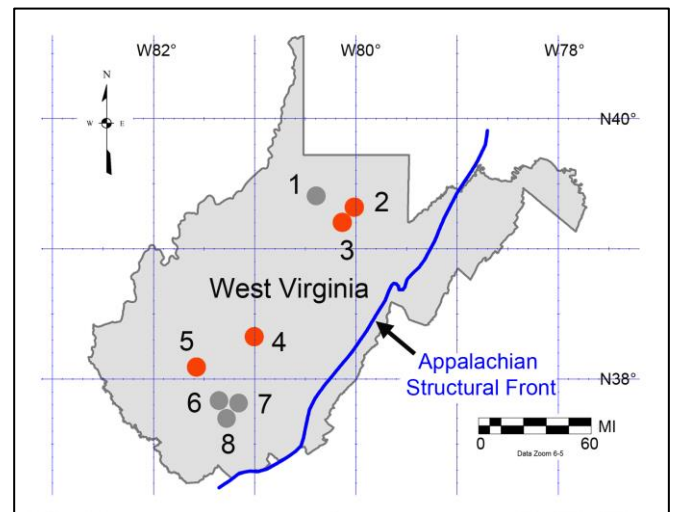


**Figure 1. Test results from Mines 2, 3, 4, 5, are cited in this paper.**

The rock core measurement concept is based in principle on the Diametrical Core Deformation Analysis (DCDA) method used over the last several years in a number of Pacific Rim drilling projects and elsewhere (Ito, Funato, Shono, 2012; Funato and Ito, 2017). The DCDA method provides stress relief direction and differential stress magnitude ( $S_H - S_h$ ) (Ito, et al, 2013). To determine absolute stress magnitude requires another stress method to provide either  $S_H$  or  $S_h$ .

The diametral method used for this study incorporates additional features that are being tested for absolute value determinations of deformation and strain ( $\epsilon_H$ ,  $\epsilon_h$ ). Two features that are improvements over the DCDA method are

direct calculation of the major and minor axes of deformation, and a procedure to identify and correct for partial truncation of the major axis of diametral elongation during the coring process in sedimentary rocks.

### DIAMETRICAL MEASUREMENT SYSTEM

A specialized benchtop hardware and software system was developed to measure and evaluate diametral variation in rock cores across 360°. Core samples are cradled and slowly turned on two horizontal drive rollers that are synchronized with a timing belt powered by a high-torque, low RPM motor. As illustrated in **Figure 2** a pair of diametrically opposed digital indicator gages, each equipped with a roller stylus, acquire uninterrupted 360° position.

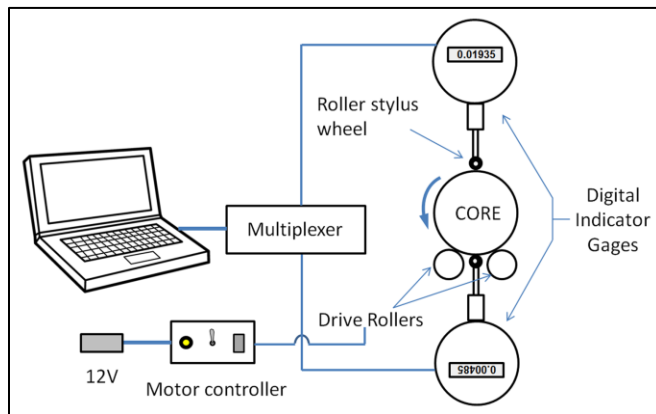


**Figure 2. Schematic of the diametral measurement device.**

The gages work in tandem to eliminate the possibility of errors related to roller/core position. The gages are each rated at 2.54 microns and gage-pair calibrations are performed using an invar steel round bar machined to a known diameter, with corrections for temperature. Data collection is performed at less than one (1) RPM constant speed for five (5) uninterrupted core revolutions. Measurement profiles are typically spaced 0.1-foot apart along the core axis. The measurement device was configured to accommodate cores ranging one (1) inch to eighteen (18) inches in length, and between one (1) inch and four (4) inches in width (diameter). The cores tested were all either two (2) inches or two and one half (2.5) inches in diameter. **Figure 3** shows an example plot of measured diameter vs azimuth, illustrating the parameters  $D_{max}$  (maximum diameter) and  $D_{min}$  (minimum diameter). The azimuth of maximum strain is in the direction of the maximum diametral elongation ( $D_{max}$ ) that results from stress relaxation (after Ito, Funato, Shono, 2012).

### SUBJECT ROCK CORES

For this study drilling operations were not altered significantly from normal practices, although some core

handling refinements were implemented. Whenever possible approximately 400 feet of core were boxed from each hole, usually beginning at the water table. Once cores were removed from the core barrel and air-dried they were not allowed to be re-wetted and were transported to a designated dry-storage location at the end of each shift.

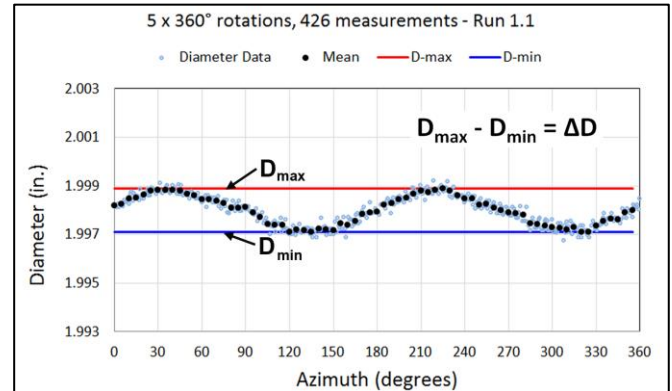


**Figure 3. Example diametral variation diagram (chart form is adapted from Ito and Funato, 2012).**

One important procedural change was to provide drill operators with re-sealable plastic bags and a suitable plastic container with a lid in order to catalogue and save any core length that remained after the box it was supposed to fit into had become completely full. Further, all smaller fragments of core were saved and placed at their proper depth location in the boxes. This was to facilitate the ability to piece together core breaks in the lab in order to maximize continuity. Diamond drilling normally produces exquisitely smooth and uniform cores, although a small percentage (about 2%) may be rugose or gouged due to rod slap, re-drilling of slipped core, a worn-out drill bit, core barrel jams, etc. All cores are assessed for such defects during sample cleaning and preparation.

Prior to testing, rock cores were air-dried at 45-55% humidity and a selection of lithologies were weighed daily until there was no further weight change due to moisture loss, at which point testing commenced.

### ORIENTING CORES WITH NORTH

Establishing a datum line for true north on rock cores was accomplished with the aid of an acoustic televiewer (ATV) summary log. As core holes were completed geophysical logs were run for resistivity, natural gamma, gamma density and ATV. All four logs are important for successfully orienting cores with a true north datum because the boxed core and the ATV log can differ from one another by a few feet. The depths for ATV logs and gamma logs on the other hand are generally in close agreement and so were used to synchronize depths between the ATV log and physical core with correlative stratigraphic features; for example sharply-

defined contacts of dissimilar rock layers that are identifiable both in core and in the gamma density log.

A standing column of water and an open core hole (no drill rods) are requirements for the ATV log. It employs a rotating sensor that transmits ultrasound pulses towards the borehole wall, recording the amplitude of the reflected signal and the travel time back to the receiver, producing a digital image (Goodfellow, et al, 2017). The tool can orient itself with respect to true north and a horizontal plane, and the resulting digital image map of the borehole is interpreted by trained operators who identify the dip angle and dip azimuth for discrete planar fractures. Fractures with dip angles greater than 25° that can be confidently correlated between the core and ATV log are used as “index fractures” to transfer a true-north datum to the core. Core continuity is improved if the driller saves all core surplus and pieces, maximizing the length of core that may be oriented from a given index fracture.

### DETERMINATION OF HORIZONTAL STRAIN AND STRESS

Core drilling removes a circular column of rock in ten to twenty foot sections, releasing it from confinement which initiates diametral elongation that is greatest in the direction of the major axis of in situ horizontal strain and stress. The expansion should initiate immediately, resulting in some lost diametral dimension until the bit cutting surface passes by, which takes just a few seconds, and the core continues upward into a protective core barrel.

The core holes drilled in this study were vertical so that diametral stress relief is horizontal. The direction of maximum diametral elongation (the major axis) and the minimum diametral elongation (the minor axis) are mutually perpendicular. For this paper the maximum horizontal stress is abbreviated  $S_H$  and the minimum horizontal stress is  $S_h$  (after Engelder, 1993). The abbreviations  $\mathcal{E}_H$  and  $\mathcal{E}_h$  refer to the principal axes of strain.  $S_H$  and  $\mathcal{E}_H$  are both oriented with the direction of maximum horizontal stress.

Two notable improvements over the DCDA method include (1) direct calculation of the major and minor axes of deformation, and (2) a procedure to identify and compensate for truncation of a portion of the major axis during the coring process. These are presented next, using the data related to the diametral variation diagram given in **Figure 3**. Unless otherwise noted the discussion that follows pertains to improvements developed by the author for strain and stress determination by the diametral method.

#### Calculating Horizontal Strain

Performing deformation calculations from the diametral measurements is the first step in determining horizontal strain. The “as-measured” diametral data is first organized

and averaged into 5° circumferential increments, giving 72 diameters of “working data,”  $D_\theta$ . The value of  $D_{min}$  is next subtracted from each value of working data to obtain values of differential diameter, which are each converted to a radius whose non-zero end point is plotted in rectangular coordinates using Equations 1a, 1b, 1c. The use of uppercase “D” and uppercase “R” signifies the values are based on “as-measured” data values.

$$\Delta R_\theta = \frac{D_\theta - D_{min}}{2} \quad (1a)$$

$$x = (\Delta R_\theta) \cos \theta \quad (1b)$$

$$y = (\Delta R_\theta) \sin \theta \quad (1c)$$

The resulting 0 to 360° plot gives a “quasi-lemniscate” figure whose minor axis equals zero and whose major axis is equal to  $D_{max} - D_{min} = \Delta D$  (see **Figure 4A**). It is a graphic representation of the database of values used to calculate diametral deformation. The diametral method proceeds with construction of a series of 3-point rosette models (after Obert and Duvall, 1967) using Equations 2a, 2b, but with units of deformation,  $U$ .

$$U_p = \frac{u_1 + u_2 + u_3}{3} + \frac{\sqrt{2}}{3} \sqrt{(u_1 - u_2)^2 + (u_2 - u_3)^2 + (u_3 - u_1)^2} \quad (2a)$$

$$U_q = \frac{u_1 + u_2 + u_3}{3} - \frac{\sqrt{2}}{3} \sqrt{(u_1 - u_2)^2 + (u_2 - u_3)^2 + (u_3 - u_1)^2} \quad (2b)$$

A series of twelve (12) 3-point deformation rosette models are constructed to evaluate deformation from 0 to 360° along the perimeter of the quasi-lemniscate figure. The first model (0°, 120°, 240°) is shown as an example in **Figure 4B**. The location of legs  $U_1$ ,  $U_2$ ,  $U_3$  relative to vertices  $A$ ,  $B$ ,  $C$  are given in **Figure 4C**. Each model gives a solution for the major and minor axes of deformation magnitude ( $U_p$  and  $U_q$ , respectively) and the major axis orientation  $\theta_p$ , which are together represented in **Figure 4B** with an ellipse oriented in the direction of the maximum horizontal stress ( $S_H$ ). Haas, 1982 gives the conditional statements needed to evaluate whether the calculated  $\theta_{pq}$  is in the direction  $S_H$  or  $S_h$ .

The major axis of deformation  $U_p$  is in the direction of maximum horizontal stress ( $S_H$ ), and perpendicular to the minor axis  $U_q$ . A radially equiangular 3-point rosette model is constructed at every 10° of arc, repeating after 120° so that the full 360° is represented by twelve (12) such models. The directions and magnitudes of the respective major and minor deformation axes for the twelve (12) elliptical models are averaged and expressed as a composite major axis length  $\bar{U}_p$  at a converted azimuth angle of  $\bar{\theta}_p$  (which is in the direction of  $S_H$ ) and a

composite minor axis length  $\bar{U}_q$  (which is in the direction of  $S_h$ ). For graphic representation the quasi-lemniscate figure is fitted with visible nodes every  $10^\circ$  of arc in preparation for an important later step.

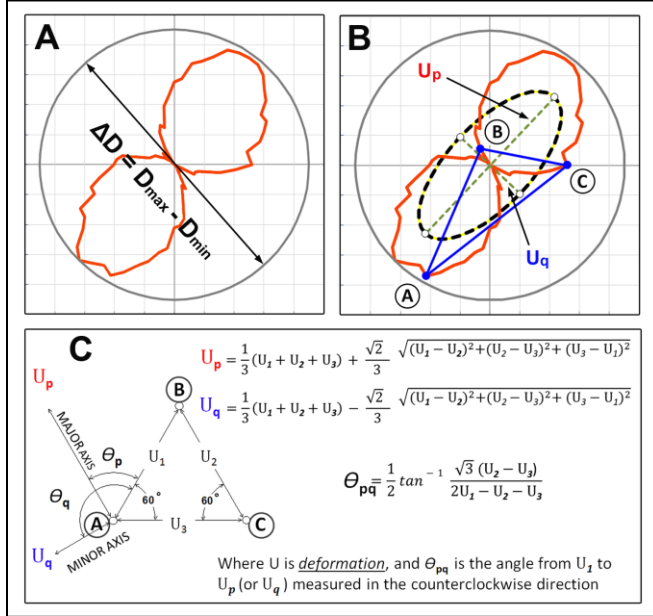


**Figure 4. Calculating deformation from differential diameter using the diametral data shown in Figure 3.**

Next, a similar but “theoretical” differential diameter model is constructed, based on the force balance equations behind Mohr’s Circle, using the “as-measured”  $D_{max}$  and  $D_{min}$  terms (note: the portion of Equation 3a in parenthesis is *after* Funato and Ito, 2017). Just as with the as-measured model each theoretical differential diameter is converted to a radius whose non-zero end point is plotted in rectangular coordinates using Equations 3b, 3c. The composite theoretical differential diameter model is used to determine how much, if any, of the major axis elongation was truncated as a result of the coring process.

The diametral variation diagram in **Figure 3** is close to sinusoidal in shape, but not perfectly so. We continue with its underlying data as the example for determining if an adjustment to  $D_{max}$  is needed. This is to compensate for major axis truncation that may have occurred during the initial few seconds of the coring process until the cutting surface of the coring bit (0.3 inches or less) has passed through a given core increment (0.1 inches or less). The adjustment does not affect the direction of  $U_p$ , but it does affect the procedure for determining stress magnitude.

The physical plot of the “theoretical” differential diameters from 0 to  $360^\circ$  for each  $5^\circ$  of arc gives a lemniscate figure similar to the quasi-lemniscate, but more uniform. The figure expresses the expected profile

of elastic diametral expansion based on the as-measured values of diameters  $D_{max}$  and  $D_{min}$ , angle  $\theta$ , and angle  $\alpha$  (the circumferential reference angle  $\theta_p$  between  $U_1$  and  $U_p$ , as shown in Figure 4C). As before, the 3-point rosette models repeat after  $120^\circ$ . The use of lowercase “r” in  $\Delta r_\theta$  signifies we are calculating the “theoretical” values this time.

$$\Delta r_\theta = \frac{\left( \frac{D_{max} + D_{min}}{2} + \frac{D_{max} - D_{min}}{2} \cos 2(\theta - \alpha) \right) - D_{min}}{2} \quad (3a)$$

$$x = (\Delta r_\theta) \cos \theta \quad (3b)$$

$$y = (\Delta r_\theta) \sin \theta \quad (3c)$$

The “theoretical” lemniscate figure is next fitted with nodes at  $10^\circ$  intervals and superimposed onto its “as-measured” counterpart for comparison. In **Figure 5A** the red and black figures show the as-measured and theoretical differential diameters, respectively. They are a reasonably close match, however by performing a series of iterations to Equation 3a, increasing the value of  $D_{max}$  each time, we can improve the fit slightly. This improved fit is presented in **Figure 5B**. The iterations increase  $D_{max}$  for the theoretical figure, only, until the  $10^\circ$  nodes in the proximal region of the black and red figures converge.

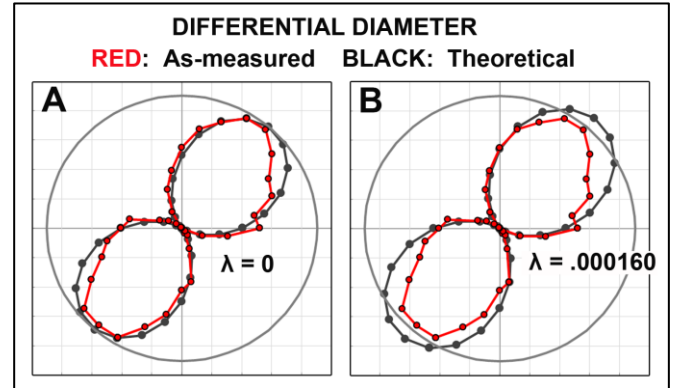


**Figure 5. The theoretical model is used to estimate the length of missing major axis dimension, expressed as “λ.”**

The amount of  $D_{max}$  stretch needed to achieve a “best fit” is expressed as the quantity  $\lambda$  (lambda), where  $D_{max} + \lambda = D'_{max}$ . The adjustment is illustrated by the total amount the adjusted major axis of the theoretical (black) figure extends outside the  $\Delta D$  gray reference circle. In this example  $\lambda = .000160$  inches. Deformation is recomputed after replacing  $D_{max}$  with  $D'_{max}$  in Equation 3a, then evaluating the deformation model once again with twelve (12) 3-point rosette models using the data series represented by the theoretical lemniscate (black) figure in **Figure 5B**.

It is the abundance of detailed  $360^\circ$  diametral data which makes this correction to  $D_{max}$  possible. This is illustrated

further using a different example (**Figure 6**) that is missing a significant portion of its expected major axis elastic elongation dimension (**Figure 6A**). The correction factor  $\lambda$  is determined as before by first constructing a radial plot of the as-measured differential diameter (the red, quasi-lemniscate figure in **Figure 6B**). It is next superimposed by its theoretical differential diameter counterpart (the black lemniscate figure) calculated from Equation 3a using the as-measured value of  $D_{max}$  ( $\lambda = 0$ ). The second step involves increasing the value of  $D_{max}$  within the theoretical model in steps until as shown in **Figure 6C** its profile converges with the superimposed as-measured model while its major axis lobes extend well outside the  $\Delta D$  perimeter. This represents the total correction length needed to restore  $D_{max}$ , which in this example is  $\lambda = .001567$  inches. In practice this procedure must be evaluated both with computational and graphic models.

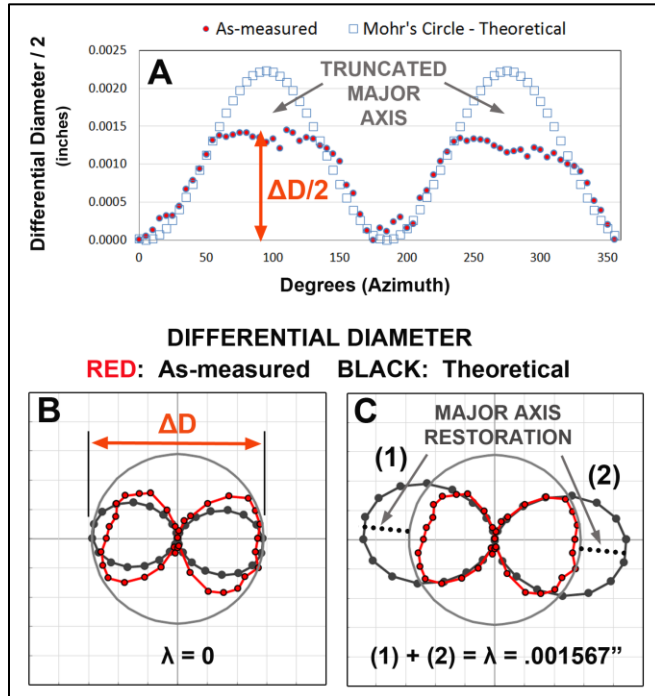


**Figure 6. An example of significant truncation to further illustrate how the as-measured diametral profile may be corrected for missing major axis dimension.**

To finish with the original example, the average magnitudes of the final major and minor principal axes of deformation are designated  $\bar{U}'_p$  and  $\bar{U}_q$ , respectively. The minor principal axis in this example needs no adjustment. Dividing each by  $D_{min}$  according to Equations 4a, 4b provides the estimated values for strain magnitude, with  $D_{min}$  used as the equivalent original diameter term in the same manner as Ito, Funato, Shono, 2012, and Funato and Ito, 2017.

$$\epsilon_H = \frac{\bar{U}'_p}{D_{min}} \quad (4a)$$

$$\epsilon_h = \frac{\bar{U}_q}{D_{min}} \quad (4b)$$

The final evaluated strain results for the **Figure 3** example data appear in **Figure 7**. The major and minor principal strains are .000660 in./in. and .000236 in./in., respectively. Although the overall profiles of an elliptical model compared to a hippopedal model are different, their principle horizontal strain axes are of the same direction and magnitude. The ratio between the major and minor axes in this example is 2.80. This includes the lambda ( $\lambda$ ) correction of .000160 inches and  $D'_{max}$  in the final run of calculations. The direction of the major axis of strain is  $42^\circ$  azimuth and is the direction of maximum horizontal stress,  $S_H$ .

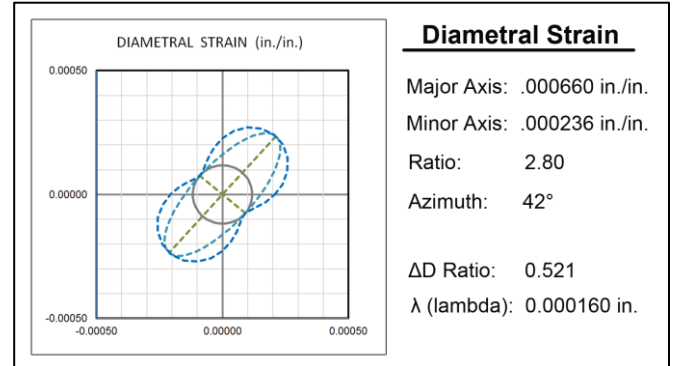


**Figure 7. Diametral strain statistics related to the data charted in Figure 3.**

The term “ $\Delta D$  ratio” (delta-D ratio) is beyond the scope of this paper, but mentioned here because it provides a useful independent estimate of the amount of expected truncation in  $D_{max}$ . For example, a diametral profile with a perfect, symmetrical sinusoidal profile that requires no  $\lambda$  correction will have a  $\Delta D$  ratio equal to 0.500. Test samples that are suitable candidates for uniaxial testing to determine their elastic modulus parameters generally exhibit  $\Delta D$  ratios that are between .475 and .625.

### Calculating Horizontal Stress

The equations used to compute the major and minor axes of stress ( $S_H$  and  $S_h$ ) are given in Equations 5a, 5b, respectively, which are valid for small deformations in material that is homogeneous, linearly elastic, and continuous. The stress values for a set of comparison downhole overcore results to be presented later include horizontal stress due to self-weight of the overlying rock strata and the Poisson Effect (Equation 5c), (after Amadei and Stephansson, 1997) but for the diametral method calculations this term is omitted (after Engelder, 1993).

$$S_H = \frac{E}{1-\nu^2} (\varepsilon_H + \nu\varepsilon_h) + (S_{hsw}) \quad (5a)$$

$$S_h = \frac{E}{1-\nu^2} (\varepsilon_h + \nu\varepsilon_H) + (S_{hsw}) \quad (5b)$$

$$S_{hsw} = \frac{\nu}{1-\nu} pgz \quad (5c)$$

With respect to Equations 5a and 5b the strain terms  $\varepsilon_H$  and  $\varepsilon_h$  are defined by Equations 4a, 4b. The parameters  $E$  and  $\nu$  refer to Young's Modulus and Poisson's Ratio, respectively. The customary means of determining their values is by destructive uniaxial compressive strength (UCS) testing methods. With respect to Equation 5c the terms  $p$ ,  $g$ , and  $z$  refer to rock wet density, the gravity constant, and depth, respectively.

One advantage of the diametral method is it affords the opportunity during UCS sample selection to visually and analytically inspect the cores for compliance with the suitability criteria of homogeneity and also  $\Delta D$  ratio. Another advantage is several diametral profiles can be merged to correspond to a specific length of test core. Test sample length is generally 2 to 2.5 times the core diameter, so to determine a composite profile three to five individual strain profiles are selected (1,200 to 2,200 diametral measurements) within the sample length from which composite strain values are computed that represent the full core length for each UCS test sample.

In the next section some practical applications are presented, beginning with a comparison of stress magnitude diametral method results from Mine 2 with six (6) corresponding stress tests performed by the downhole overcoring method.

## COMPARISON WITH OVERCORE IN-SITU STRESS RESULTS AND A PREDICTIVE STRESS MODEL

### MINE 2: Stress magnitude

Mine 2 is located in the north central part of West Virginia (see **Figure 1**) where cores from seven (7) coreholes were tested and a large database was compiled. Approximately 260 linear feet of cores were tested in 0.10-foot increments, from depths ranging 300 feet to 1,100 feet. Diametral profiles were compiled for approximately 2,400 increments of oriented core, representing approximately 1,000,000 pairs of gage readings. Useable results were obtained for 719 increments, many of which were combined, contributing 394 samples to the database of strain azimuth and magnitude for Mine 2.

Downhole overcoring tests were performed in two of the core holes by an independent geotechnical consulting firm, providing six (6) sets of in situ horizontal stress results. Parallel tests using the diametral method were performed on

six (6) corresponding core samples from the same holes and from similar depths that were selected for lithologic similarity to, and closest proximity with, the overcore test samples.

Linear regressions comparing those results appear in **Figure 8A** for the major axis stress ( $S_H$ ), and in **Figure 8B** for the minor axis stress ( $S_h$ ). The diametral method stress results are compared with: (1) downhole overcoring stress relief test results, and (2) results from a predictive model, referred to here as the Mark/Gadde (M/G) model (Mark and Gadde, 2010).

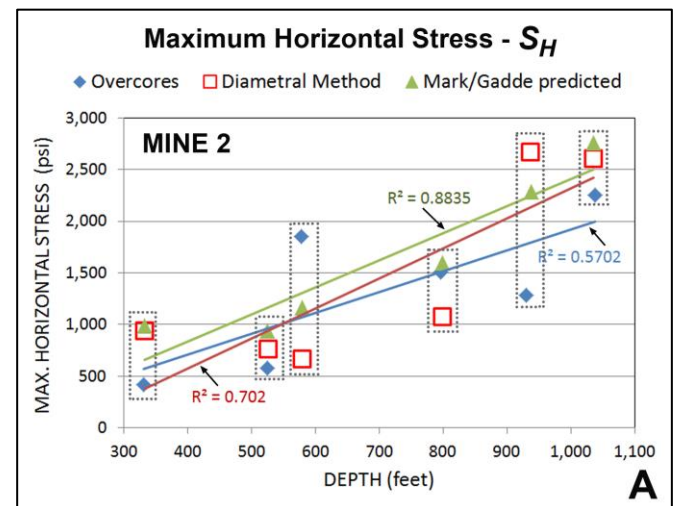


**Figure 8A. Major axis stress magnitude using the Diametral Method (red squares) compared with two other methods.**

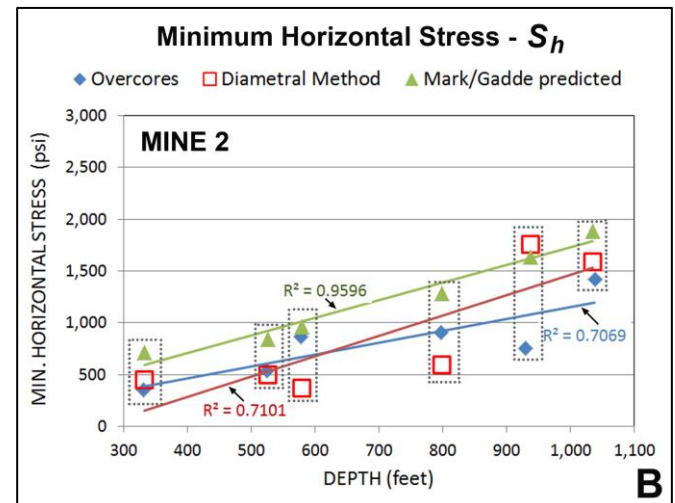


**Figure 8B. Minor axis stress magnitude using the Diametral Method (red squares) compared with two other methods.**

The apparent agreement between the average of the stress magnitude results by the diametral method and the overcore method is 90.6% (major axis) and 91.8% (minor axis). Stress

varies with depth, but the gradient is linear and the comparison depths for the respective sample sets were basically the same.

The M/G model for the Eastern U.S. coalfields is given in Equations 6a, 6b (imperial units). The model is derived from more than 350 stress measurements from underground coal mines (42 of those measurements are from Eastern U.S. coal mines), which treats depth and elastic modulus as independent variables in regression analysis (Mark and Gadde, 2010).

$$S_H = -298 + 1.64(\text{Depth}) + .000410(E\_Modulus) \quad (6a)$$

$$S_h = 0 + 1.34(\text{Depth}) + .000150(E\_Modulus) \quad (6b)$$

The apparent agreement between the average results for the computed values of absolute stress magnitudes by the diametral method and M/G model is 89.5% (major axis) and 71.8% (minor axis).

As illustrated in **Figures 8A, 8B** the linear regression results for the diametral method lie midway between the overcore results and the M/G model results.

There is a caveat to the above comparisons involving the elastic modulus parameters. The overcore stress results had been computed with secant values for Young’s Modulus, and slight adjustments had been made to the ASTM values for Young’s Modulus for five of the six samples. For consistency in comparisons the diametral method and M/G predictive models use those same modulus values when computing stress.

The *stress/depth* slope gradient for the diametral results is consistent with the overcore results and the M/G estimate. In other locations where the M/G model was compared to the diametral method their slope gradients were also similar. Their stress magnitude values were similar about 50% of the time, with the remainder achieving approximate agreement using a simple multiplier that was the same for both  $S_H$  and  $S_h$ . This is not unexpected as the M/G model is essentially a statistical average from a database of regional stress measurements, for which the diametral method stress/depth gradients are similar, but the diametral method computed stress magnitudes and its charted y-intercepts are site-specific.

The most extreme examples of deviation from the M/G model were found in diametral method results involving the Eagle seam roof and floor strata for two (2) mines, where stress magnitude results using the diametral method were consistently lower than the M/G prediction by a multiplier factor of 1.4 to 2.5. The reason behind this phenomenon of very low horizontal stress magnitude is still under study.

The *direction* of maximum horizontal stress ( $S_H$ ) is of great importance for mine planning. The diametral method makes acquisition of large and statistically robust datasets practical, which is important for characterizing the direction of maximum horizontal stress. This is put to good use next where rock type, relative rock strength, and the direction of maximum horizontal stress were found to be closely related at Mine 2 and the nearby Mine 3, which operate in an area with a history of cutter roof and related horizontal stress issues. A collection of 17 independent downhole overcore tests performed previously at those mines show a 92° azimuth range for the direction of the maximum horizontal stress ( $S_H$ ). The diametral method was used to investigate this apparent anomaly.

### MINE 2- Stress direction ( $S_H$ azimuth)

The large database of directional strain data compiled for Mine 2 provides evidence of an association between the maximum horizontal stress ( $S_H$ ) direction and rock strength, for which lithology is an indicator. Histogram plots of azimuth frequency for  $S_H$  were initially organized strictly according to rock type among the three principal lithotypes sandstone (SS), sandy shale (SSH), shale (SH), but it was found that organizing according to relative rock strength may be more appropriate.

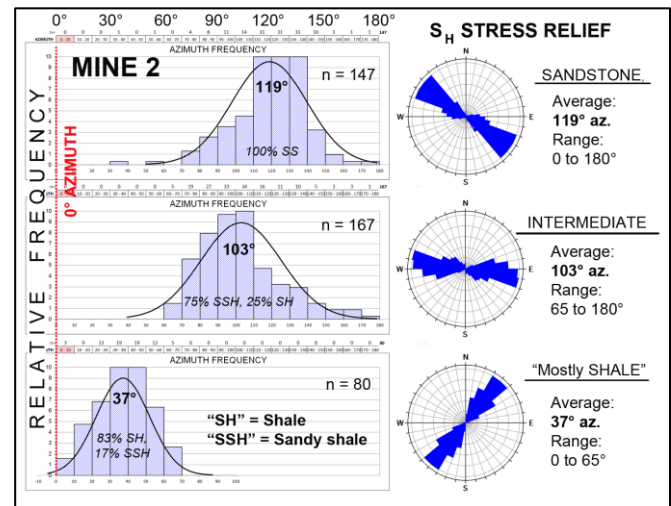


**Figure 9. Mine 2: Diametral Method maximum horizontal stress ( $S_H$ ) azimuth frequency histograms fall into three normal distributions, each dominated by a particular lithology. The same data is summarized in rose diagrams.**

As shown in **Figure 9** the  $S_H$  trends at Mine 2 comprise three (3) normally distributed groups. The group exhibiting the highest mean  $S_H$  azimuth contains 100% sandstone. The lowest  $S_H$  azimuth values were exhibited in predominantly shale rocks. “Intermediate” rocks exhibit a continuous series between shale and sandstone rocks, with corresponding

intermediate mean  $S_H$  azimuth. However, the distinction between shale and sandy shale can be subjective, and lithology is an imperfect metric for relative rock strength. After considerable study it was found to be more appropriate to first view the SSH and SH populations together, then separate their apparent bimodal distribution at the 65° bar increment. The result was two groups which each approximated a normal distribution, but with some cross-over of SSH and SH between groups. The resulting classification according to this approach is shown in **Figure 9** for which the intermediate group is comprised of 75% SSH, 25% SH, and the group labeled “mostly shale” was comprised of 83% SH, 17% SSH. The rose diagrams on the right of the figure present the same data in a different view to further illustrate graphically the association between maximum horizontal stress ( $S_H$ ) azimuth and rock properties. Additional study continued with the nearby Mine 3 where corroboration with the Mine 2 results was found.

### MINE 3- Stress direction ( $S_H$ azimuth)

Mine 3 is located approximately 8 miles southwest of Mine 2 (see **Figure 1**) and exhibits a similar range of overburden lithologies, but with a higher percentage of shale rocks than Mine 2. Analysis of the Mine 3 data is based on three (3) holes, from which approximately 50 linear feet of cores were tested between depths of 363 and 730 feet. Diametral profiles were compiled for 464 increments of oriented core, representing approximately 220,000 pairs of gage readings. Useable strain results were acquired for 367 increments.

As was done with Mine 2 the data for Mine 3 were initially sorted strictly by lithology, where it is also found that the sandstone (SS) rocks comprise one normal distribution, and the shale (SH) and sandy shale (SSH) rocks together exhibit a bimodal distribution (similar to Mine 2). When separated at the 65° bar increment the result was two groups which each approximated a normal distribution (again, similar to Mine 2); one comprised of 92% SH, 8% SSH rocks (**Figure 10**), the other was comprised of 50% SH, and 50% SSH.

The mean azimuths of maximum horizontal stress ( $S_H$ ) for each of the three (3) rock classifications are strikingly similar to Mine 2. Also, both mines show a counter-clockwise rotation of the mean azimuth when moving from the sandstone class to the shale class. Their respective 95% confidence intervals of mean  $S_H$  azimuth for each of the normal distributions is generally +/- 3°, except for the intermediate rocks at Mine 3 which is +/- 5°. Because there is considerable random variation due to rock anisotropy and other variables the standard deviation is rather large, ranging 11.5° to 21.0°. This underscores the importance of working with a statistically robust population of samples to cut through random variation to determine the mean  $S_H$  azimuth.

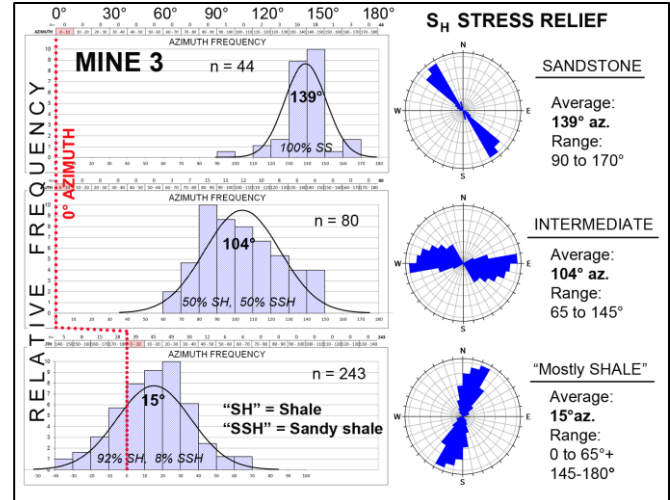


**Figure 10. Mine 3: Diametral Method maximum horizontal stress ( $S_H$ ) azimuth frequency histograms fall into three normal distributions, each dominated by a particular lithology. The same data is summarized in rose diagrams.**

For completeness **Figure 11** is included to show the azimuth relationships of maximum horizontal stress ( $S_H$ ) when the data are organized strictly by lithology.

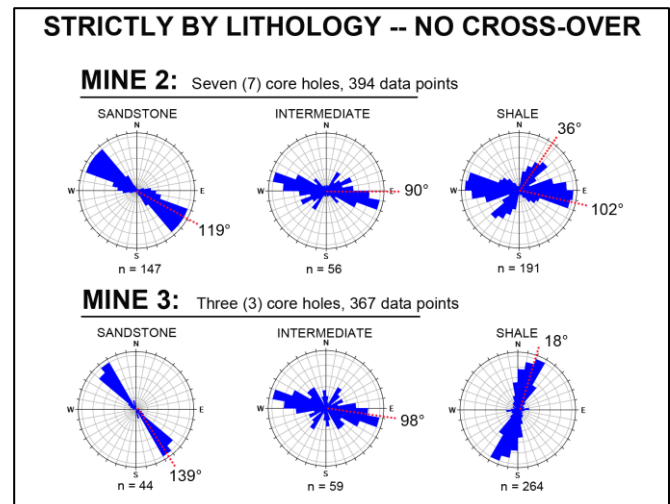


**Figure 11. Diametral Method comparisons for Mine 2 and Mine 3 are also similar when maximum horizontal stress ( $S_H$ ) azimuth is organized strictly by lithology.**

While the rose diagrams are similar in many respects to the **Figures 9** and **10** views there are clusters of data, in particular a significant bimodal split in the “shale category” for Mine 2, that on closer inspection is due to lithology cross-over related to differences in rock strength that lithologic description alone does not capture. For that reason later studies generally include Brinell hardness tests (Boutrid, et al, 2013) for each measurement profile to help in quantifying and characterizing the crossover.

These diametral method results for Mines 2 and 3 represent perhaps the widest range of  $S_H$  azimuth variance among different rock types so far observed in West Virginia. Shale rocks exhibit the lowest  $S_H$  azimuths, compared to other sedimentary rocks, which tend to be aligned parallel to the axes of nearby anticline fold structures. The contemporary maximum horizontal stress ( $S_H$ ) azimuths exhibited in shale rocks in proximity to the Appalachian Structural Front (see **Figure 1**) are believed to be strongly influenced by a rock fabric attributed to post-Alleghanian release fractures that impart a preferred direction of weakness in shales, facilitating the opening of joints during stress relaxation or reorientation (Evans, et al, 1989). Release fractures develop in response to the removal of overburden during erosion (Engelder, 1985).

Extensional joints are often used as stress direction indicators as they propagate in the direction of maximum horizontal compressive stress ( $S_H$ ) at the time they form (Pollard and Segall, 1987). Researchers have observed from cross-cutting relationships of joints in outcrops that silty rocks generally fracture before shale (Engelder, 1985), while at the same time (during the Alleghanian orogeny) the horizontal compressive stress field in West Virginia was undergoing counter-clockwise rotation (Evans, 1994). The observed diversity in maximum horizontal stress ( $S_H$ ) azimuths may be related to these mechanisms.

### MINE 2 and MINE 3: The combined dataset

The combined datasets for Mines 2 and Mine 3 total 761 samples (see **Figure 12**) which summarizes the available diametral data for this mining district into one view, comprised of three (3) normal distributions, illustrating the strong association between rock properties and the azimuth of maximum horizontal stress ( $S_H$ ) direction. Their respective mean  $S_H$  azimuths are 123°, 102°, and 21°, corresponding to the sandstone group (100% SS), the intermediate group (66% SH, 34% SSH), and the least competent “mostly shale” group (90% SH, 10% SSH), respectively. The 95% confidence interval is +/- 3° or less. Standard deviations are 21° for all categories.

There is a 21° difference in  $S_H$  azimuth between the competent sandstone rocks and intermediate rocks, and an 81° difference between intermediate and the least competent rocks, comprised mostly of shale. This represents a 102° range between the respective mean  $S_H$  azimuths for sandstone and shale. This is in general agreement with previous estimates of the maximum horizontal stress ( $S_H$ ) directions operative during Stage 2: “Main Phase” of the Alleghanian orogeny, through Stage 4: “Post Alleghanian release jointing” when the compressive stress field was

undergoing a continuous counter-clockwise rotation (Evans, 1994). This perspective, and the diametral method results, help explain why a combined dataset of independent Mine 2 and Mine 3 downhole overcore stress results similarly show a wide range of  $S_H$  azimuths that varies with rock properties. This is discussed next in a final comparison.

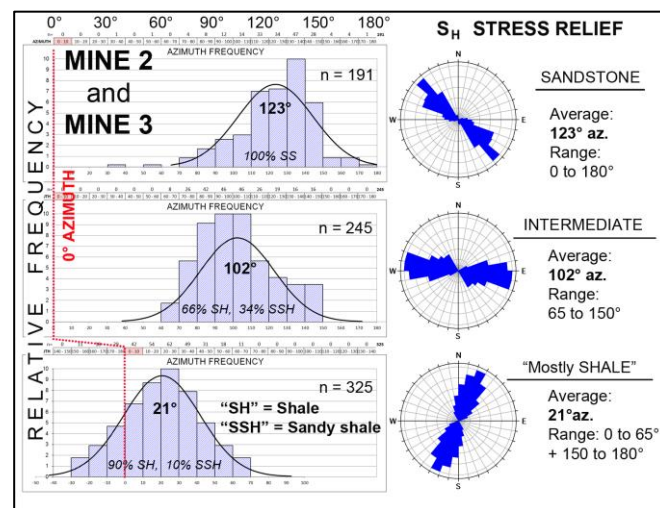


**Figure 12. Mines 2 and 3 (combined): Diametral Method maximum horizontal stress ( $S_H$ ) azimuth frequency, for the combined data shown in Figure 9 and Figure 10.**

### MINE 2 and MINE 3: Comparison with 17 overcores

A dataset of 17 independent overcore horizontal stress test results for Mine 2 and Mine 3 show maximum horizontal stress  $S_H$  spread across a wide range of azimuths (see **Figure 13A**) which increase generally with increasing uniaxial compressive strength (UCS).

Samples that were described as shale exhibit UCS values generally less than 11,000 psi, while those described as sandy shale or sandstone generally exhibit UCS values greater than 11,000 psi (see **Figure 13B**). In addition to their higher UCS values the sandstone and sandy shale overcore test samples as a group exhibit the highest values for  $S_H$  azimuth. Conversely, the shale overcore test samples, which have comparatively low UCS values, as a group comprise most of the observed lower values for  $S_H$  azimuth. There are also a few lithology cross-overs with UCS, as expected. These results are consistent with diametral method results.

Further, the range of  $S_H$  azimuth results for the 17 overcore test results illustrated in **Figure 13B** (31° to 123°) is similar to the range of mean  $S_H$  azimuths for the diametral results illustrated in **Figure 12** (21° to 123°). This represents an azimuth range of 92° for the overcoring test results and 102° for the diametral method results, supporting the contention that the wide range in the overcore  $S_H$  azimuths is real.

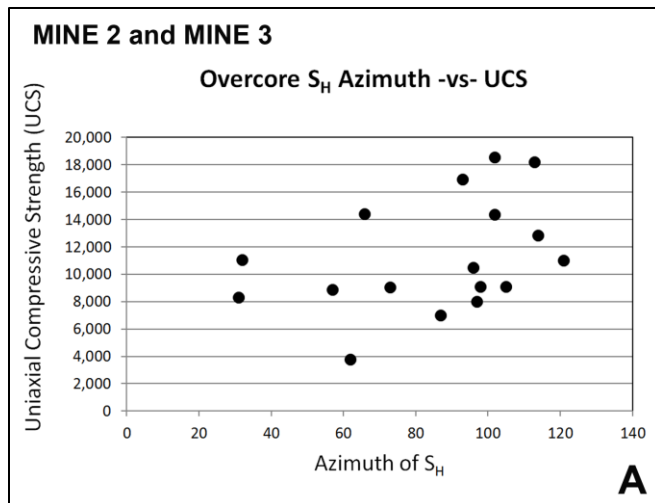


Figure 13A. Overcore data showing the azimuth of maximum horizontal stress direction increases with UCS.

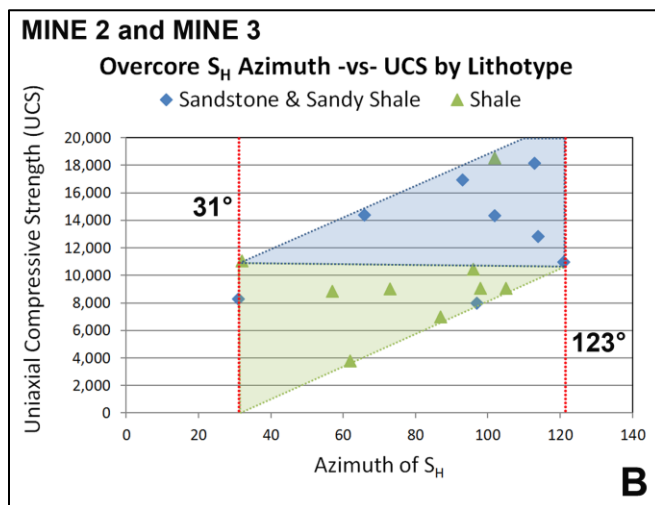


Figure 13B. Overcore data showing UCS generally increases with the sandy content of the rock core samples. The  $S_H$  azimuth range ( $31^\circ$  to  $123^\circ$ ) is nearly identical to the Diametral Method results ( $21^\circ$ - $123^\circ$ ) shown in Figure 12.

The dilemma for mine engineers however remains with the question, “Which maximum horizontal stress direction should I use?” In the case of Mine 2 and Mine 3 the answer seems to be two-tiered. Part of the answer lies in classification of the rock by both lithology and rock strength, for which this mining district now has corresponding  $S_H$  azimuths. It is already understood that strain magnitudes vary by rock type. One might also need to consider the shear and detachment effects of competing horizontal stress relief slip directions at bedding contacts of dissimilar rock types. It is also fair to ask the question, “Are the azimuths of  $S_H$  for diametral method results in the direction of the contemporary horizontal stress field, or are they reflective of a paleo stress that is different?” This question is addressed in

the next section, which compares the diametral method results with two (2) independent contemporary maximum horizontal stress direction indicators.

### CORROBORATION OF THE DIAMETRAL METHOD RESULTS BY TWO OTHER $S_H$ INDICATORS OF THE CONTEMPORARY HORIZONTAL STRESS DIRECTION

#### MINE 4- Stress direction ( $S_H$ azimuth) comparison with drilling-induced *petal-centerline fractures*

It is desirable to compare stress results with other methods to provide a measure of consistency and reliability (Amadei and Stephansson, 1997). At Mine 4 a series of *induced hydraulic fractures* provide independent verification of the direction of maximum horizontal stress ( $S_H$ ) as determined by the diametral method in massive sandstone.

Hydraulic fractures are a type of extension fracture that may be used to infer the direction of the maximum horizontal compressive stress ( $S_H$ ) at the time they formed. These fractures opened naturally in the distant past at great depth where local fluid overpressure conditions exist; or today at more shallow depths when induced pressures from drilling operations exceed the local minimum in situ stress. In this latter case the strike of fracture propagation indicates the direction of the *contemporary* maximum horizontal stress ( $S_H$ ). At Mine 4 this principle is used to demonstrate that the diametral method is reporting the local contemporary  $S_H$  direction.

From one (1) core hole at Mine 4 approximately 63 linear feet of cores were tested, in 0.10-foot increments, from depths ranging 311 to 588 feet. Diametral profiles were compiled for 541 increments of oriented core, representing approximately 225,000 pairs of gage readings. Useable strain results were acquired for 193 increments, some of which were combined, contributing 102 samples to the diametral method database for strain azimuth and magnitude at Mine 4.

As shown in **Figure 14**, the combined data ( $n = 102$ ) are normally distributed about a mean of  $59^\circ$  azimuth which is in approximate alignment with the presumed horizontal stress direction for the area. All lithologies are combined into a histogram of relative azimuth frequency.

The rose diagrams in **Figure 14** summarize  $S_H$  azimuth frequency according to lithology. Approximately equal numbers of sandstone and intermediate samples were tested, with little if any differences in their indicated azimuths of maximum horizontal stress ( $S_H$ ). Shale samples were few in number but indicate  $S_H$  direction deviates  $18^\circ$  in the counter clock-wise direction (the same rotation direction exhibited for shale at Mines 2 and 3).

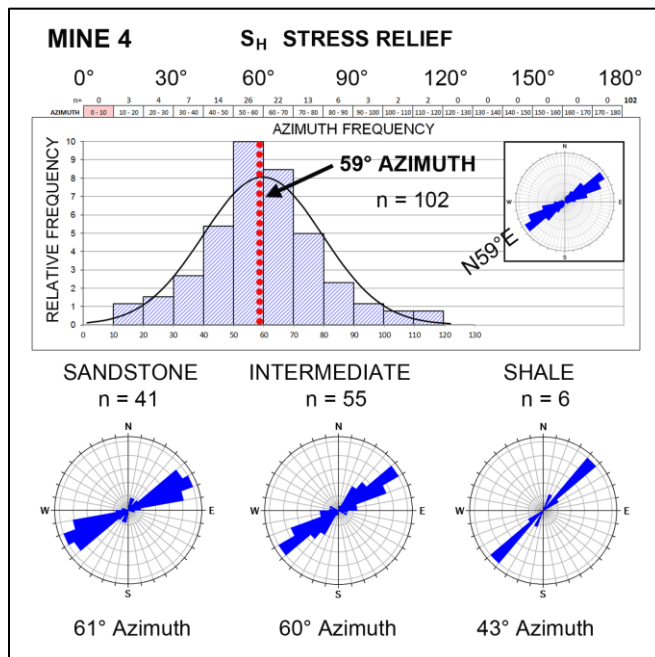


**Figure 14. MINE 4: Diametral Method azimuth frequency for the maximum horizontal stress (all lithologies combined) is normally distributed about 59° azimuth.**



**Figure 15. MINE 4: One of three drilling-induced petal-centerline (P-C) fractures that corroborate the Diametral Method results are aligned with the inferred contemporary maximum horizontal stress direction.**

A series of three (3) drilling-induced petal-centerline (P-C) fractures are recorded both in the rock core and in the ATV log at depths 337.7 to 343.3 feet (see **Figure 15**). P-C fractures are useful in providing corroboration of the maximum horizontal stress direction (Kulander and Dean, 1990). Their orientation is controlled exclusively by in situ stress rather than by the reorientation of stress following stress relief (Engelder, 1993).

The diametral method measurements show a low stress relief condition that facilitated fracture opening. This is mentioned because in other locations where tectonic (natural) fractures exist or P-C (induced) fractures were created, stress relief was also found to be anomalously low. P-C fractures initiate when drilling-induced pressures in the borehole exceed the minimum in-situ horizontal stress, propagating a vertical planar crack ahead of the core bit during drilling that is oriented in the direction of maximum horizontal stress ( $S_H$ ).

The P-C fractures at Mine 4 occurred in massive sandstone and opened along an average strike of 63° azimuth. This is in agreement with the nearest diametral method results in un-fractured sandstone where the local  $S_H$  direction is 61° azimuth. This supports the conclusion that the major axis of stress relief for the diametral method is in the contemporary maximum horizontal stress ( $S_H$ ) direction.

### **MINE 5- Stress direction ( $S_H$ azimuth) comparison with drilling-induced borehole breakouts**

Mine 5 is located approximately 35 miles southwest of Mine 4. It operates in the same seam as Mine 4 and has similar overburden lithology. The direction of maximum horizontal stress ( $S_H$ ) indicated by the diametral method results was found to be in close agreement with the inferred  $S_H$  direction from two borehole breakouts at this location.

Borehole breakouts (see **Figure 16**) are compression-induced shear fractures that propagate axially along opposite sides of the borehole wall in response to flattening of the borehole by the local contemporary maximum horizontal stress,  $S_H$ . Breakout sets align horizontally in the direction of the minimum horizontal stress,  $S_h$ , which is by definition perpendicular to  $S_H$  compression. Breakouts appear in the borehole wall, but not in the core samples.

The ATV log shows an upper set of borehole breakouts at 583 feet depth which indicates the local  $S_H$  direction is 117° azimuth. A lower breakout set identified at 629 feet depth indicates the local  $S_H$  direction is 115° azimuth (i.e., average 116°); (see **Figure 16**). A robust dataset of 387 diametral strain profiles compiled for this 46-foot interval between the two breakout horizons indicates the mean  $S_H$  direction is 113° azimuth, with a standard deviation of 21° and a 95% confidence interval of  $\pm 3^\circ$ . Azimuthal agreement is 3° between the measured mean  $S_H$  direction by the diametral method and the inferred  $S_H$  direction for the borehole breakout results. These results also support the conclusion that the diametral method is reporting major axis stress relief that is in the contemporary maximum horizontal stress ( $S_H$ ) direction.

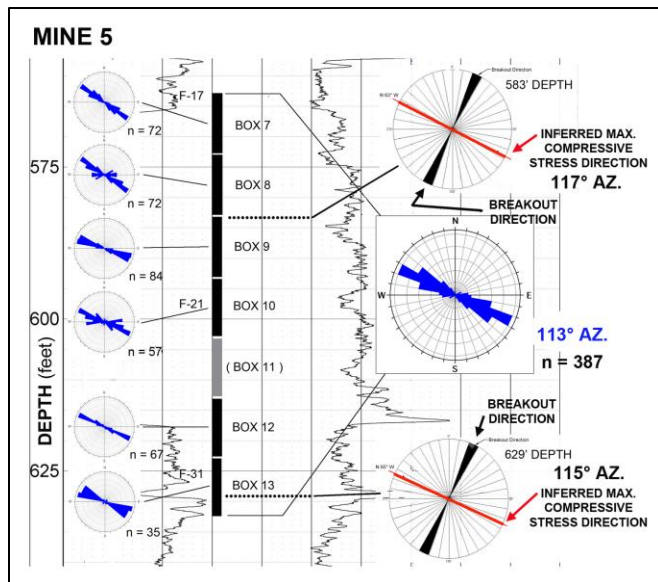


**Figure 16. Two borehole breakouts at Mine 5 corroborate the diametral method results are aligned with the inferred contemporary maximum horizontal stress direction.**

## SUMMARY

The direction of the contemporary maximum horizontal stress as determined by the diametral method is corroborated by two different stress direction indicators in massive sandstone overburden rocks at Mines 4 and 5. At Mine 4 three P-C fractures (hydraulic in origin) confirmed the maximum horizontal stress ( $S_H$ ) direction to be  $63^\circ$  azimuth, and at Mine 5 borehole breakouts (borehole flattening) confirmed the  $S_H$  direction to be  $116^\circ$  azimuth. This is within  $3^\circ$  of agreement with the diametral method results, which exhibit maximum horizontal stress ( $S_H$ ) azimuths of  $61^\circ$  and  $113^\circ$ , respectively.

At Mine 2 and Mine 3 the lithologic assemblage was more diverse. The direction of maximum horizontal stress ( $S_H$ ) exhibited in the 761 samples tested at these two mines was found to vary according to strength properties of the rocks. In sandstone rocks the mean direction of  $S_H$  was found to be  $123^\circ$  azimuth; in predominantly shale rocks the mean direction of  $S_H$  was found to be  $21^\circ$  azimuth; and in intermediate rocks the mean direction of  $S_H$  was found to be  $102^\circ$  azimuth. This agrees with seventeen (17) downhole overcoring test results at Mines 2 and 3 that show a similar range and trend in maximum horizontal stress ( $S_H$ ) azimuths, which increase as uniaxial compressive strength (UCS) values and sandy content of the rock increase.

These findings using a diametral deviation method for stress estimation illustrate that on a bed unit scale the in-situ horizontal stress can vary in a systematic way with lithology and rock strength. The phenomenon could be related to a continuous rotation in the compressive stress direction

during evolution of the Alleghanian orogeny which imprinted extensional fractures as stress signatures in different rock layers at different times. Stress direction and magnitude are closely dependent upon the properties of the rocks.

## CONCLUSIONS

The diametral method presented here provides the means to estimate in-situ horizontal strain and stress in advance of mining by evaluating common rock cores in 360 degrees using direct-contact diametral measurement and deformation rosette model techniques. With minor exceptions it is both non-destructive and non-invasive and does not slow down drilling operations or mining operations. The results presented here show general agreement of horizontal stress direction and stress magnitude with parallel overcore test results. The results also demonstrate close agreement of contemporary horizontal stress ( $S_H$ ) direction with other stress direction indicators, including drilling-induced hydraulic fractures and borehole breakouts. The diametral method can provide large, statistically robust datasets for estimating local horizontal strain and stress in an economical way that is unprecedented. The diametral method as presented is found to give reliable estimates of the direction of horizontal stress and relative strain magnitude. Estimation of absolute strain magnitude remains a work in progress.

## ACKNOWLEDGEMENTS

Thanks are extended to the contract drillers and company geologists, engineers, and managers whose dedication and cooperation made this study possible.

## REFERENCES

- Amadei, B. and Stephansson, O. 1997. *Rock Stress and Its Measurement*. London, UK, Chapman & Hall: 75, 96.
- Boutrid, A., Bensehamdi, S., Chaib, R. 2013. Investigation into Brinell hardness test applied to rocks, *World Journal of Engineering*: 10(4): 369-382.
- Engelder, T. 1985. Loading paths to joint propagation during a tectonic cycle: an example from the Appalachian Plateau, U.S.A. *Structural Geology*, v. 7, Nos. 3-4: 459-476.
- Engelder, T. 1993. *Stress Regimes in the Lithosphere*. Princeton, N.J., Princeton University Press: xxi, 172, 305.
- Evans, K. F., Oertel, G., and Engelder, T. (1989). "Appalachian stress study 2. Analysis of Devonian shale core: Some Implications for the nature of contemporary stress variations and Alleghanian deformation in Devonian rocks." *Journal of Geophysical Research: Solid Earth*. 94(B6): 7155-7170.

- Evans, M. 1994. Joints and decollement zones in Middle Devonian shales: Evidence of multiple deformation events in the central Appalachian Plateau. *Geological Society of America*. Bulletin 106(4): 447-460.
- Funato, A., and Ito, T. 2017. A new method of diametrical core deformation analysis for in-situ stress. *International Journal of Rock Mechanics and Mining Sciences*, vol. 91: 112-118.
- Goodfellow, S. D., Simser, B., Drielsma, C., Gerrie, V. 2017. Underground Mining Technology – M. Hudyma & Y. Polvin (eds). *Australian Centere for Geomechanics*: 487-496.
- Haas, C. J. 1982. Basic Tools for Deformation Measurements in Mines. Chap. 7.3.3, *Underground Mining Methods Handbook*, W.A. Hustrulid, ed., SME, Littleton, CO: 1506–1511.
- Ito, T., Funato, A., Shono, T. 2012. Laboratory Verification of the Diametrical Core Deformation Analysis (DCDA) Developed for In-Situ Stress Measurements. 46<sup>th</sup> U.S. Rock Mechanics/Geomechanics Symposium, *American Rock Mechanics Association*: 12-588.
- Ito, T., A. Funato, Lin, W., Doan, M.-L., Boutt, D. F., Kano, Y., Ito, H., Saffer, D., McNeill, L. C., Byrne, T., and Moe, K. T. 2013. Determination of stress state in deep subsea formation by combination of hydraulic fracturing in situ test and core analysis: A case study in the IODP Expedition 319, *J. Geophys. Res. Solid Earth*, 118: 1203–1215.
- Kulander, B., Dean, S., Ward, Jr., B. 1990. Fractured Core Analysis: interpretation, logging, and use of natural and induced fractures in core. AAPG Methods in Exploration Series, No. 8, Tulsa, Oklahoma, *American Association of Petroleum Geologists*.
- Mark, C., Gadde, M. 2010. Global trends in coal mine horizontal stress measurements, in Aziz, N (ed). 10<sup>th</sup> Underground Coal Operators' Conference, *University of Wollongong & the Australasian Institute of Mining and Metallurgy*, 2010: 21-39.
- Obert, L., Duvall, W. 1967. *Rock Mechanics and the Design of Structures in Rock*. John Wiley and Sons: 42, 411.
- Pollard, D.D., Segall, P. 1987. Theoretical displacements and stresses near fractures in rock: with applications to faults, joints, veins, dikes, and solution surfaces. In: Atkinson, B. (Ed.), *Fracture Mechanics of Rock*. Academic Press, Orlando, FL: 227–350.